NASA TECHNICAL MEMORANDUM

NASA TM X-71695

NASA TM X-71695

(NASA-TM-X-71695) SOLAR COLLECTOR PERFORMANCE EVALUATION WITH THE NASA-LEWIS SOLAR SIMULATOR-RESULTS FOR AN ALL-GLASS-EVACUATED-TUBULAR SELECTIVELY-COATED COLLECTOR WITH A DIFFUSE G3/44

N75-31568

Unclas
35060

SOLAR COLLECTOR PERFORMANCE EVALUATION WITH THE NASA-LEWIS SOLAR SIMULATOR - RESULTS FOR AN ALL-GLASS-EVACUATED-TUBULAR SELECTIVELY-COATED COLLECTOR WITH A DIFFUSE REFLECTOR

by Frederick Simon
Lewis Research Center
Cleveland, Ohio
April 1975

SOLAR COLLECTOR PERFORMANCE EVALUATION WITH THE NASA-LEWIS SOLAR SIMULATOR - RESULTS FOR AN ALL-GLASS-EVACUATED-TUBULAR SELECTIVELY-COATED COLLECTOR WITH A DIFFUSE REFLECTOR

by Frederick Simon

Lewis Research Center

E-8289

ABSTRACT

An evacuated tubular all-glass solar collector was tested in the NASA-Lewis solar simulator for inlet temperatures of 70° to 200° F, flux levels of 230 and 345 Btu/(hr)(ft^2), a coolant flow rate of 7 lb/(hr)(ft^2), and incident angles of 0°, 33°, and 52°. Test results plotted in a form suggested by analysis indicate a very low heat loss coefficient. The collector shows excellent performance on an all-day performance basis, and also for conditions corresponding to temperatures required in solar Rankine systems and/or for low flux level radiation.

INTRODUCTION

An area being investigated by the Lewis Research Center in its efforts to improve the technology of alternate energy sources is solar energy for the heating and cooling of buildings. An important component of a building solar heating and cooling system is the solar collector. The objective of the solar collector test program at LeRC is to determine which types and designs of collectors have the best potential to be efficient, economical and reliable.

One approach for obtaining collectors which can be efficient at the relatively high ($\sim 200^{\circ}$ F) temperatures required for solar cooling and solar Rankine systems is to reduce the thermal radiation and convection losses. Reduction of thermal radiation losses by the use of a solar selective surface has been reported (ref. 1). One of the ways in which convection losses may be significantly reduced in collectors is by the use of vacuum between the absorbing surface and the glazing. The present paper reports the test results with the LeRC solar simulator of an all-glass tubular collector which employs a selective surface and a vacuum for reducing collector thermal losses.

The particular collector used in these tests was obtained from the Owens-Illinois Corporation. This is the first evacuated-tube type of solar collector that became available for test. Whether or not this one collector design provides performance that is representative of the general class of evacuated solar collectors cannot be determined until similar tests are carried out on other specific evacuated collectors as they become available for test.

Collector Description

A photograph of the collector tested is shown in figure 1. This collector is an Owens-Illinois Model SEC100-3. It is an all-glass evacuated, nonfocusing, nontracking tubular collector. The collector shown in figure 1 consists of twelve $41\frac{1}{2}$-inch long tubes (length exposed to sun-the bottom of the collector. The total area available for solar energy collection (essentially the area of back reflector) is 14.35 square feet. Each tube of the collector consists of an inner tube of 41 mm diameter placed within an outer tube of 51 mm diameter. The inner tube through which the liquid flows is coated with a selective coating with an absorptance of about 0.8 and an emittance of about 0.09. The annular region between the inner and outer tube is evacuated to a vacuum sufficient to prevent convection and conduction thermal losses. The transmittance of the cover tube relative to the absorber tube cross section is 0.91. This transmittance takes into account the variation of transmittance with respect to direct radiation about the curved surface of the outer tube. Figure 2 shows how the collector might be installed in a practical situation. Collector tubes are placed in both sides of the manifold with the roof acting as the reflector surface. (Photograph in fig. 2 supplied by Owens-Illinois.)

EXPERIMENTAL METHOD AND FACILITY

A drawing and a photograph of the facility are presented in figures 3 and 4. The primary components of the facility are the energy source (solar simulator), the liquid flow loop, and the instrumentation and data acquisition equipment. A summary of information describing the facility is presented in table I. More detailed information on the facility and its use is given in references 2 and 3.

Solar Simulator

The basic rationale for the use of a solar simulator for the testing of solar collectors was given in reference 4. This approach allows for controlled conditions that makes it possible to properly compare the performance of different collector types. The simulator shown in figure 3 consists of 143 tungsten-halogen 300-watt lamps placed in a modular array with Fresnel lenses placed at their focal distance so as to collimate the radiation. A comparison of spectral characteristics of the simulator output with air mass-2 sunlight is given in table II. Table II demonstrates that the solar simulator does an adequate job of simulating the sun's radiation.

Coolant Flow Loop

The flow loop consists of storage and expansion tanks, pump, heater, test collector, and the required piping shown schematically in figure 5. The hot fluid storage tank is a commercially available water heater for home use. The tank has two electrical immersion heaters, 5 kilowatts each, and has a capacity of 80 gallons. The pump is a gear type unit driven by a 1/4 horsepower electric motor through a variable speed drive.

A heat exchanger using city water as a coolant is used to control the temperature of the collector coolant fluid at the collector inlet.

A 50/50 by weight mixture of ethylene-glycol and water is used in the liquid loop. The specific gravity of the mixture is checked with a precision grade hydrometer. To suppress vapor formation the entire flow loop is pressurized to approximately 15 psig by applying a regulated inert gas pressure to the top of the expansion tank.

The collector to be tested is mounted on a support stand that allows rotation about either the horizontal axis or the vertical axis. This permits variation of the incident angle of the radiant energy to simulate both seasonal and daily variations, if desired.

Instrumentation and Data Acquisition

The parameters needed to evaluate collector performance are: liquid flow rate, liquid inlet and outlet temperatures, the simulated solar flux, wind speed, and the ambient temperature. The flow rate is determined with a calibrated turbine-type flow meter that has an accuracy better than one percent of the indicated flow. The collector inlet and outlet temperatures are measured with ISA type E thermocouples (chromel-constantan). The thermocouples were calibrated at

32° and 212° F. The error in absolute temperature measurement is less than 1° F and the differential temperature error between the inlet and outlet thermocouples was less than 0.2° F.

The ambient temperature is measured with an ISA type E thermocouple mounted in a radiation shield. The simulated solar flux is measured with a water-cooled Gardon type radiometer having a sapphire window. The radiometer was calibrated with a National Bureau of Standards irradiance standard.

The millivolt-level electrical outputs of the measuring instrument are recorded on magnetic tape by the use of a high speed data acquisition system. The information from the tape is sent to a digital computer for data reduction and computation. The computer results are printed out in the test facility within minutes after the data is initially recorded.

Test Procedure

The collector was mounted on the test stand (fig. 1) so that the radiant flux was either normal or at different incident angles to the collector. To achieve the correct simulation of the sun's position with respect to the collector, it was necessary to vary both the tilt angle (angle between collector plane and horizontal) and the angle of the rotation of the test stand about the vertical axis. These two angles were varied so that different incident angles could be obtained and still have the simulator flux vector perpendicular to the collector tube axes.

The present tests were run at incident angles of 0°, 33°, 52°, and corresponding tilt angles of 57°, 29.5°, and 27.8°. For the evacuated tube collector there was no effect on performance as a result of changing tilt angle due to the presence of a vacuum between the absorber surface and the outer tube. The coolant flow rate was adjusted to a value of 7 pounds per hour per square foot of total collector area. This flow rate was the highest flow rate that could be achieved without exceeding a pressure limit for this collector of approximately 7 lb/in.^{2}. Before the simulator was turned on the collector was given time to achieve thermal equilibrium at the inlet temperature chosen (1 hr or more). After thermal equilibrium was established for a given inlet temperature the simulator was turned on and the desired radiant flux was obtained by adjusting the lamp voltage. After steady-state conditions occurred, usually in 30 minutes, data was recorded. The radiant flux was then readjusted to a second value at the same collector inlet temperature, steady-state conditions obtained, and data again recorded. This procedure was followed at a given inlet temperature for the three incident angles chosen. The collector inlet temperature was then set to another value and the procedure repeated.

Analytical Method

Because of the unique nature of the evacuated-tubular collector, when compared to conventional collectors, it is worthwhile to analyze its performance to make possible a correct interpretation of the experimental findings. Figure 6 shows the collector with the key variables which determine its performance. The analysis shows the importance of the incident angle of the incoming radiation, the diffuse reflector, the area available for direct radiation compared to the area available for diffuse energy from reflector, etc.

The basic equation for the collector heat balance is:

$$Q_u = Q_{A,DR} + Q_{A,DF} - Q_L \tag{1}$$

Where $Q_{A,DR}$, the amount direct radiation absorbed is:

$$Q_{A,DR} = N q_{DR} D_a L_t \alpha\tau \tag{2}$$

and $Q_{A,DF}$, the amount diffuse radiation absorbed is produced when the direct radiation passes between the tubes and strikes the diffuse reflector in back of the tubes. This "window" for the direct radiation varies with the incident angle. The width (w) of the sunlit portion of the diffuse reflector is related to the incident angle as follows:

$$w = D_o\left[2.0 - 1.0/\cos\theta_i\right] \tag{3}$$

It can be seen that this width will equal zero for an incidence angle of 60^{o} which is a good practical limit for all early morning and late afternoon solar collection.

The total amount of diffuse radiation reflected is then:

$$Q_{DF} = Nq_{DR} \cos \theta_i w L_t \rho \tag{4}$$

The amount of this energy which reaches any particular tube is a function of the total view factor from all the sunlit strips on the diffuse reflector to a particular tube. This total view factor will vary with tube position, but it will be assumed not to vary for the present analysis. Assuming that the absorptance and the transmittance is the same as for the direct radiation, the total background diffuse energy absorbed is:

$$Q_{A, DF} = Nq_{DR} \cos \theta_i w L_t \rho \mathcal{F} \alpha \tau \tag{5}$$

Where $\mathcal{F}$ is equal to the sum of the view factors from all the sunlit strips to a tube

$$\mathcal{F} = \Sigma F_{w-t} \tag{6}$$

The last term of equation (1) is the collector heat loss (Q_L). Assuming uniform heat loss around tube circumference

$$Q_L = N\pi D_a L_t(\overline{T}_s - T_a)U_L \tag{7}$$

Combining equations (7), (5), and (2) with equation (1) gives

$$Q_u = A_{DR}\left[\alpha\tau q_{DR} R - \pi U_L(\overline{T}_s - T_a)\right] \tag{8}$$

where

$$A_{DR} = ND_a L_t \tag{9}$$

and

$$R = 1 + \frac{D_o}{D_a}(2\cos\theta_i - 1)\rho f \tag{10}$$

(R represents the ratio of total radiation to direct radiation.) The efficiency is defined as

$$\eta = Q_u / q_{DR}\cos\theta_i A_T \tag{11}$$

Where A_T is the total reflector area. Combining equations (11) and (8)

$$\eta = \frac{A_{DR}}{A_T}\left[\frac{\alpha\tau R}{\cos\theta_i} - \frac{\pi U_L(\overline{T}_s - T_a)}{q_{DR}\cos\theta_i}\right] \tag{12}$$

Equation (12) needs to be expressed in terms of an easily measurable quantity, such as the fluid inlet temperature (T_i). To do this we need to first determine the flux of the useful energy (q_u). Assuming that the heat transfer to the tubes can be expressed in terms of an overall heat transfer coefficient (U),

$$q_u = \frac{Q_u}{A_{DR} + A_{DF}} = U(\overline{T}_s - \overline{T}_f) \tag{13}$$

Combining equations (12) and (13) and eliminating $\overline{T}_s$, gives

$$\eta = \frac{A_{DR}}{A_T} F'\left[\frac{\alpha\tau R}{\cos\theta_i} - \frac{\pi U_L(\overline{T}_f - T_a)}{q_{DR}\cos\theta_i}\right] \tag{14}$$

where

$$F' = 1 \Bigg/ \left[1 + \frac{A_{DR}}{A_{DR} + A_{DF}} \frac{\pi U_L}{U}\right] \tag{15}$$

Expressing equation (14) in terms of a variable fluid temperature and variable useful energy

$$Q_u(x) = \frac{F'A_{DR}x}{NL_t}\left[\alpha\tau q_{DR}R - \pi U_L(T_f(x) - T_a)\right] \tag{16}$$

and from equation (16) the differential of the flux can be expressed as

$$dq_u(x) = \frac{dQ_u(x)}{(A_{DR} + A_{DF})\dfrac{N\,dx}{L_t}} = -\left(\frac{A_{DR}}{A_{DR} + A_{DF}}\right)\pi U_L F'\, dT_f(x) \tag{17}$$

Expressing the useful flux in terms of the fluid energy

$$\frac{q_u(x)(A_{DR} + A_{DF})\,dx}{NL_t} = C_P G A_T\, dT_f(x) \tag{18}$$

Dividing equation (17) by equation (18)

$$\frac{dq_u(x)}{q_u(x)} = -\frac{F'\pi U_L}{C_P GNL_t}\frac{A_{DR}}{A_T}\,dx \tag{19}$$

and integrating

$$q_u(x) = q_u(x = 0)e^{-Bx} \tag{20}$$

Where $B = \frac{F'\pi U_L}{C_P GNL_t} \frac{A_{DR}}{A_T}$

Defining the average flux as

$$\bar{q}_u = \frac{1}{NL_t} \int_0^{NL_t} q_u(x)\, dx \tag{21}$$

Substituting equation (20) and integrating we obtain

$$\bar{q}_u = q_u(x = 0)\; F_R/F' \tag{22}$$

where the flow factor

$$F_R = \left(\frac{GC_P}{U_L}\right)\left(\frac{A_T}{\pi A_{DR}}\right)\left[1 - e^{-(F'U_L/GC_P)(\pi A_{DR}/A_T)}\right] \tag{23}$$

This flow factor is similar to the one obtained by Whillier for conventional flat-plate collectors (ref. 5). We set the value of $A_T/\pi A_{DR}$ in equation (23) equal to one we obtain the flow factor of Whillier. Equation (22) may be expressed as

$$Q_u = Q_u(x = 0)\; F_R/F' \tag{24}$$

Substitute equation (24) into equation (16) and using the definition for efficiency (eq. (11)) we obtain

$$\eta = \frac{A_{DR}}{A_T} F_R\left[\frac{\alpha\tau R}{\cos\theta_i} - \frac{\pi U_L(T_1 - T_a)}{q_{DR}\cos\theta_i}\right] \tag{25}$$

Equation (25) is the basic equation needed for expressing collector efficiency in terms of the inlet temperature (T_1) and the flux in the plane of the collector ($q_{DR}\cos\theta_i$).

RESULTS AND DISCUSSION

The experimental collector efficiency was calculated using the following equation:

$$\eta = C_p G(T_1 - T_0)/q_{DR} \cos \theta_i \tag{26}$$

Where $G = W/A_T$. A tabulation of collector efficiency for different inlet temperatures, simulator flux levels and incident angles is given in table III.

Performance Curves

The data of table III are plotted in the form suggested by equation (25) in figure 7. For comparison purposes the experimental curve for a selective coated, nonevacuated two-glass flat-plate collector is also shown in figure 7 (refs. 1 and 3). The more horizontal slope of the data for the evacuated collector indicates lower heat losses for this collector compared to the nonevacuated two-glass collector. The other point of interest is that in contrast to conventional flat-plate collectors, the efficiency increases with incident angle. This is due to the direct radiation being received by the tubes being independent of incident angle (up to an incident angle of 60^o). From the intersection of the correlation lines for the evacuated tubular collector with the line of the black Ni collector, it can be seen that the evacuated tubular collector is superior for conditions of high inlet temperature or low flux levels. More will be said of this later.

Collector Parameters

The slopes of the curves of figure 7 are related to the following equation as indicated by equation (25):

$$\text{slope} = -\frac{A_{DR}}{A_T} F_R \pi U_L \tag{27}$$

Equation (27) indicates that the slope is independent of incident angle which the performance curves of figure 7 confirm. By the use of equations (27), (23), and the value of the value of the slope from figure 7, the overall heat loss coefficient (U_L) can be calculated. A theoretical value of the overall heat loss coefficient can be obtained by solving the basic radiation equations with an external convection coefficient corresponding to 7 miles/hour and by including the heat loss contributed by the distribution header.

Table IV shows a comparison of the theoretical and experimental values of the heat loss coefficient. Three possible reasons for the experimental value of U_L being 30 percent higher than theory are that the vacuum level was not high enough to prevent conduction losses, uncoated glass regions, and a higher coating emissivity than expected. In any case the collector heat loss is extremely low.

From equation (25), it can be seen that the intercept values of the curves of figure 7 are given by

$$a = \frac{A_{DR}}{A_T} F_R \frac{\alpha \tau R}{\cos \theta_i} \tag{28}$$

A check of the experimental value of a may be made for an incident angle of 60°, when there is no back reflection and $R = 1.0$. The intercept (a) at 60° is calculated using equation (28) and the value of the flow (F_R) obtained with equation (27) ($F_R = 0.98$). This calculated intercept value is compared with an experimental intercept value in table V. In table V the experimental value of the intercept is given for an incident angle of 52°. At this incident angle there is very little back reflection which makes possible a comparison with the zero back reflection case ($\theta_i = 60^{\circ}$, $R = 1.0$). Table V indicates a good comparison between the calculated and experimental value of the intercept for an incident angle of 60°.

For the other incident angles used in the experiments, values of R may be calculated with equation (28) and the experimental values of the intercept (a). The relationship of the experimental values of R with the incident angles is shown in figure 8. Figure 8 with equation (25) gives the basis for calculating collector performance for different values of incident angle (θ_i) inlet temperature (T_1) and radiation flux (q_{DR}). Since the value of R represents the ratio of the total radiation to the direct radiation reaching the collector tubes, its value is an indication of the importance of the diffuse reflector in back of the tubes. Without the reflector the value of R is one as is the case for a 60^o incident angle (fig. 8). Figure 8 shows that at normal incidence the value of R is 1.64 which means that the diffuse reflector contributes 39 percent of the total energy received by the collector tubes and that this contribution decreases with increasing incident angle. At an incident angle of 60^o there is no longer any "window" for the radiation to reach the diffuse reflector and at this point R is equal to one.

Performance Comparison

In reference 3, a comparison was made of 15 solar collector types tested in the simulator. This comparison was made using the simulator results for zero incident angle. The best performer in the efficiency ranking given in reference 3 was the black-nickel two-glass nonevacuated flat-plate collector whose performance is shown as the dotted curve in figure 7.

Using the performance ranking approach of reference 3, a comparison is made in table VI between the glass evacuated tubular collector and the black-nickel two-glass collector. Table VI shows a better performance for the black-nickel, two-glass collector when compared to the tubular collector for the solar conditions used in reference 3. Since the black-nickel absorptance was 0.95, a better comparison would be made if the coating of the tubular collector also had an absorptance of 0.95.

Correcting the existing performance curve of the tubular collector for an absorptance of 0.95 we can make a prediction of an improved version of the glass tubular collector. The performance of the improved version shown in table VI indicates a better performance than the black-nickel collector at the 240° F inlet temperature condition (corresponding roughly to solar Rankine). The performance difference between the black nickel and tubular collector is not large, and one might wonder about the advantages of an evacuated collector system. One advantage, of course, is that an evacuated system gives the coating the humidity protection needed to minimize coating degradation. The performance curves of figure 7 are a strong indicator that an all-day performance comparison would probably be a better basis for judging the performance capabilities of the evacuated glass tubular collector.

By the use of all-day insolation data for a June day (for this calculation, we used data from Blue Hill, Massachusetts) for calculating collector efficiency, a better comparison can be made between the evacuated tubular and black-nickel collectors. Calculated all-day performance curves are shown in figure 9 for the inlet temperature of 200° F (corresponding roughly to absorption air conditioning). Figure 9 shows that the tubular collector is a better collector during early morning and late afternoon hours. As expected the black-nickel collector is a better collector for two hours either side of the noon hour. By taking the ratio of summation of the total available energy to the summation of the useful energy, a daily efficiency can be calculated. The results of this calculation are shown in table VII. Table VII shows that the glass tubular collector for two hours either side of the noon hour. By taking the ratio of summation of the useful energy to the summation of the available formance at inlet temperatures of 200° and 240° F. The performance of the tubular collector when based on all-day conditions becomes equal to the 200° F inlet temperature performance of the black-nickel collector, and surpasses the performance of the black-nickel collector for a 240° F inlet temperature condition. This comparison would probably be more pronounced for a low flux day in favor of the glass tubular collector.

CONCLUSIONS

An all-glass tubular collector was analyzed and tested in the NASA-Lewis solar simulator. The particular collector tested was obtained from Owens-Illinois Corporation. Tests and analysis show this collector to have a very low heat loss, and an efficiency which increases with larger incident angles, in contrast to conventional flat-plate collectors where the efficiency decreases with an increase in incident angle. This incident angle effect of the glass tubular collector, plus its low heat loss makes this type of collector a good performer at inlet temperature levels of 200° and 240° F with ambient temperature of 80° F and/or at low flux conditions. Whether or not the particular collector used in this test is representative of the general class of evacuated-tube solar collectors has not yet been determined.

REFERENCES

1. Simon, F. F.: An Evaluation Under a Simulated Sun of Two Black-Nickel Coated Flat-Plate Solar Collectors, NASA TM X-3226, 1975.

2. Vernon, R. W.; and Simon, F. F.: Flat-Plate Collector Performance Determined Experimentally with a Solar Simulator. Presented at Intern. Solar Energy Soc., Annual Meeting, Fort Collins, Color., Aug. 19-23, 1974. NASA TM X-71602.

3. Simon, F. F.: Status of the NASA-Lewis Flat-Plate Collector Tests with a Solar Simulator. Presented at NSF/RANN Collector Workshop, New York City, Nov. 1974. NASA TM X-71658.

4. Simon, F. F.; and Harlemert, P.: Flat-Plate Collector Performance Evaluation. The Case for a Solar Simulation Approach. Presented at Intern. Solar Energy Soc., Cleveland, Ohio, Oct. 3-4, 1973. NASA TM X-71427.

5. Whillier, A.: Solar Energy Collection and Its Utilization for House Heating. Sc. Thesis, Dept. Mech. Eng., Massachusetts Institute of Technology, 1953.

APPENDIX - SYMBOLS

A area, ft^2

a intercept of performance curves dimensionless

C_p heat capacity, Btu/(lb)(^oF)

D_a absorber diameter, ft

D_o outside tube diameter, ft

F_R collector flow efficiency factor, dimensionless

F radiation view factor, dimensionless

G flow per unit of total collector area, lb/(hr)(ft^2)

L length, ft

N number of tubes

Q rate of thermal energy, Btu/hr

q energy flux, Btu/(hr)(ft^2)

R ratio of total to direct radiation, dimensionless

T temperature, ^oF

U_L overall heat loss, coefficient, Btu/(hr)(ft^2)(^oF)

U overall heat transfer coefficient, Btu/(hr)(ft^2)(^oF)

W flow rate, lb/hr

w width of sunlit strip, ft

α coating absorptivity, dimensionless

η collector efficiency, dimensionless

τ transmittance

θ_i incident angle of solar radiation, deg

ρ reflectance of diffuse reflector, dimensionless

Subscripts:

A absorbed

a ambient

DF	diffuse
DR	direct
f	fluid
L	loss
o	out
S	surface
T	total
t	tube
U	useful
1	inlet
0	outlet

Superscripts:

–	average

TABLE I. - NASA-LEWIS SOLAR SIMULATOR SUMMARY

Radiation source

143 lamps, 300 W each

GE type ELH, tungsten-halogen, dichroic coating

9^{o} total divergence angle

Test area

4 by 4 ft, maximum

Test condition limits

Flux: 150 to 350 Btu/hr-ft^2

Flow: up to 1 gal/min (30 lb/hr-ft^2)

Inlet temp.: 75^{o} to 210^{o} F

Wind: 0 to 10 mph

TABLE II. - COMPARISON OF SOLAR SIMULATOR AND AIR-MASS 2 PERFORMANCE

		Air-mass-2 sunlight	Simulator
Energy output (percent)	Ultraviolet	2.7	0.3
	Visible	44.4	48.4
	Infrared	52.9	51.3
Energy uses	Absorptivity (selective surface)	0.90	0.90
	Glass transmission	.85	.86
	Al mirror reflectivity	.86	.88

TABLE III. - BASIC EXPERIMENTAL DATA; $A_T = 14.35\ FT^2$

θ_i	θ_{tilt}	Flow gal/min	G lb/(hr)(ft^2)	T_1 ^oF	T_0 ^oF	T_a ^oF	q_{DR}	$q_{DR} \cos \theta_i$ Btu/(hr)(ft^2)	η %	P_1 lb/in.^{2}	ΔP lb/in.^{2}
0	57.0	0.199	7.29	72.8	90.9	78.5	224	224	48.0	6.4	1.9
		.198	7.26	73.1	98.8	79.4	340	340	44.9	6.3	1.8
		.194	7.00	147.4	162.1	75.4	230	230	38.2	6.0	1.3
		.193	7.00	147.9	171.7	76.3	343	343	41.6	6.0	1.3
		.195	6.99	193.3	205.1	76.7	228	228	31.7	6.1	1.3
		.193	6.92	194.2	214.5	77.8	344	344	36.0	6.1	1.3
33	49.5	0.201	7.37	75.9	91.4	76.9	230	193	48.4	6.3	1.9
		.203	7.44	76.6	100.3	78.1	344	289	50.2	6.2	1.8
		.198	7.14	149.0	162.5	76.9	231	194	42.3	5.6	1.1
		.197	7.12	149.8	170.2	75.4	340	285	43.5	5.5	1.1
		.189	6.78	196.9	207.6	76.7	230	193	33.0	5.8	1.2
		.184	6.60	196.9	215.5	77.2	340	285	37.8	6.0	1.3
52.0	27.8	0.207	7.58	75.7	88.8	77.5	229	141	57.8	6.0	2.0
		.203	7.43	75.6	94.7	78.4	343	212	54.9	5.9	1.9
		.198	7.17	152.0	162.1	75.8	228	141	43.8	5.1	1.2
		.198	7.15	148.7	166.2	76.8	342	211	50.4	5.4	1.1
		.196	7.04	196.2	204.3	77.0	230	142	35.3	5.2	1.3
		.192	6.88	196.6	211.5	77.8	344	212	42.4	5.8	1.5

TABLE IV. - COMPARISON OF EXPERIMENTAL HEAT LOSS COEFFICIENT WITH THEORY

U_L (experimental)	U_L (theory) Btu/(hr)(ft^2)(^{o}F)
0.20	0.14

TABLE V. - CALCULATED AND EXPERIMENTAL INTERCEPT VALUES

a (experimental) $\theta_i = 52^o$	a (eq. (25)) $\theta_i = 60^o$
0.57	0.55

TABLE VI. - COLLECTOR PERFORMANCE COMPARISON FOR NORMAL INCIDENCE AND $q_i = 250$ BTU/(HR)(FT^2)

Collector		$T_1 = T_a = 80^o$ F percent	$T_1 = 140$ $T_a = 80$	$T_1 = 200, 120$ $T_a = 80, 0^o$ F	$T_1 = 240$ $T_0 = 80^o$ F
Black Ni-two-glass		71	60	45	34
Glass evacuated tubular collector	Present coating	45	39	34	30
	Coating with $\alpha = 0.95$	54	48	42	39

TABLE VII. - COLLECTOR PERFORMANCE (EFFICIENCY)

ON AN ALL DAY BASIS

Collector	$T_1 = 200^o$ $T_a = 80^o$	$T_1 = 240$ $T_a = 80$
Black Ni two-glass	38%	31
Glass evacuated tubular collector	38	35

E-8284

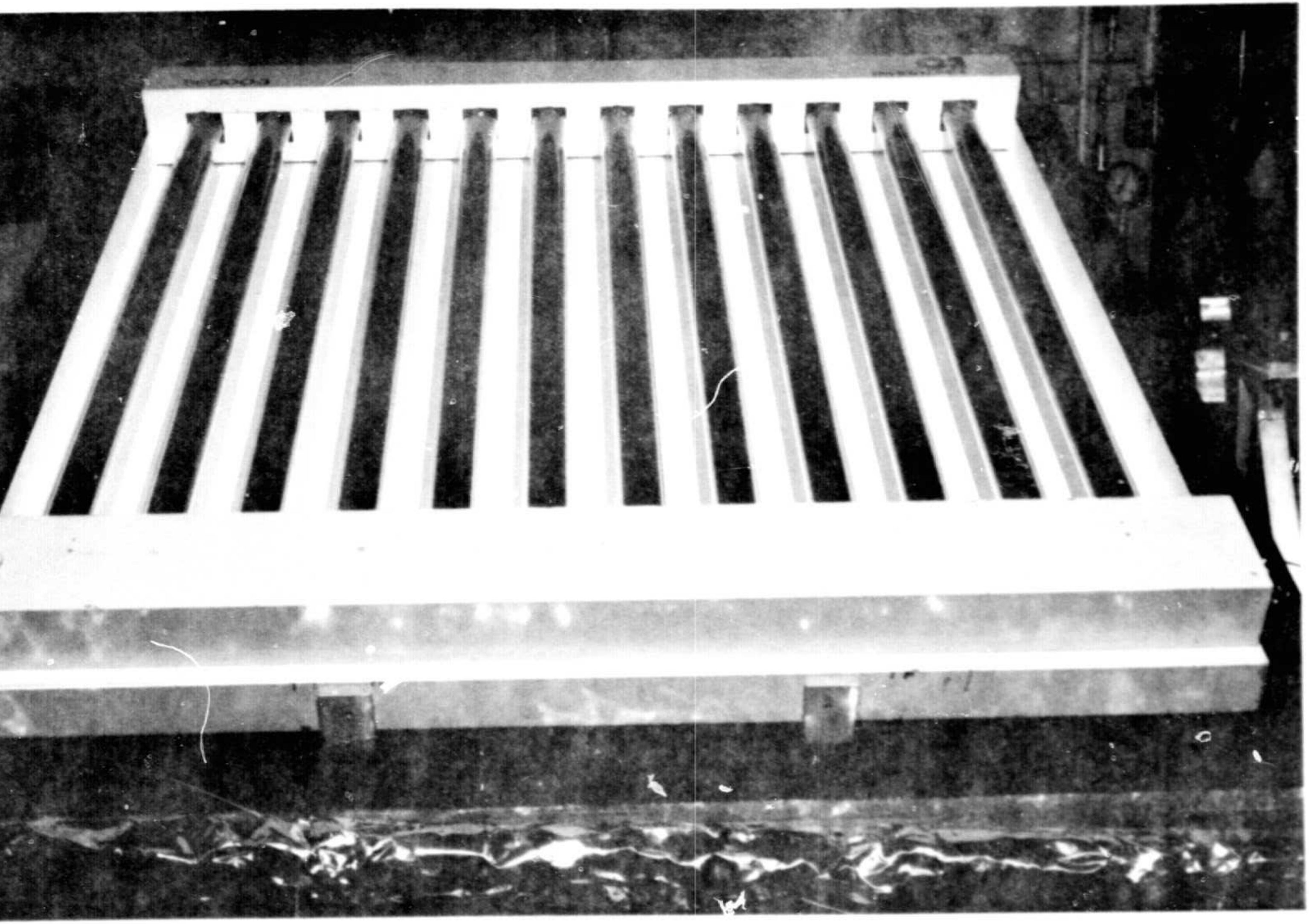

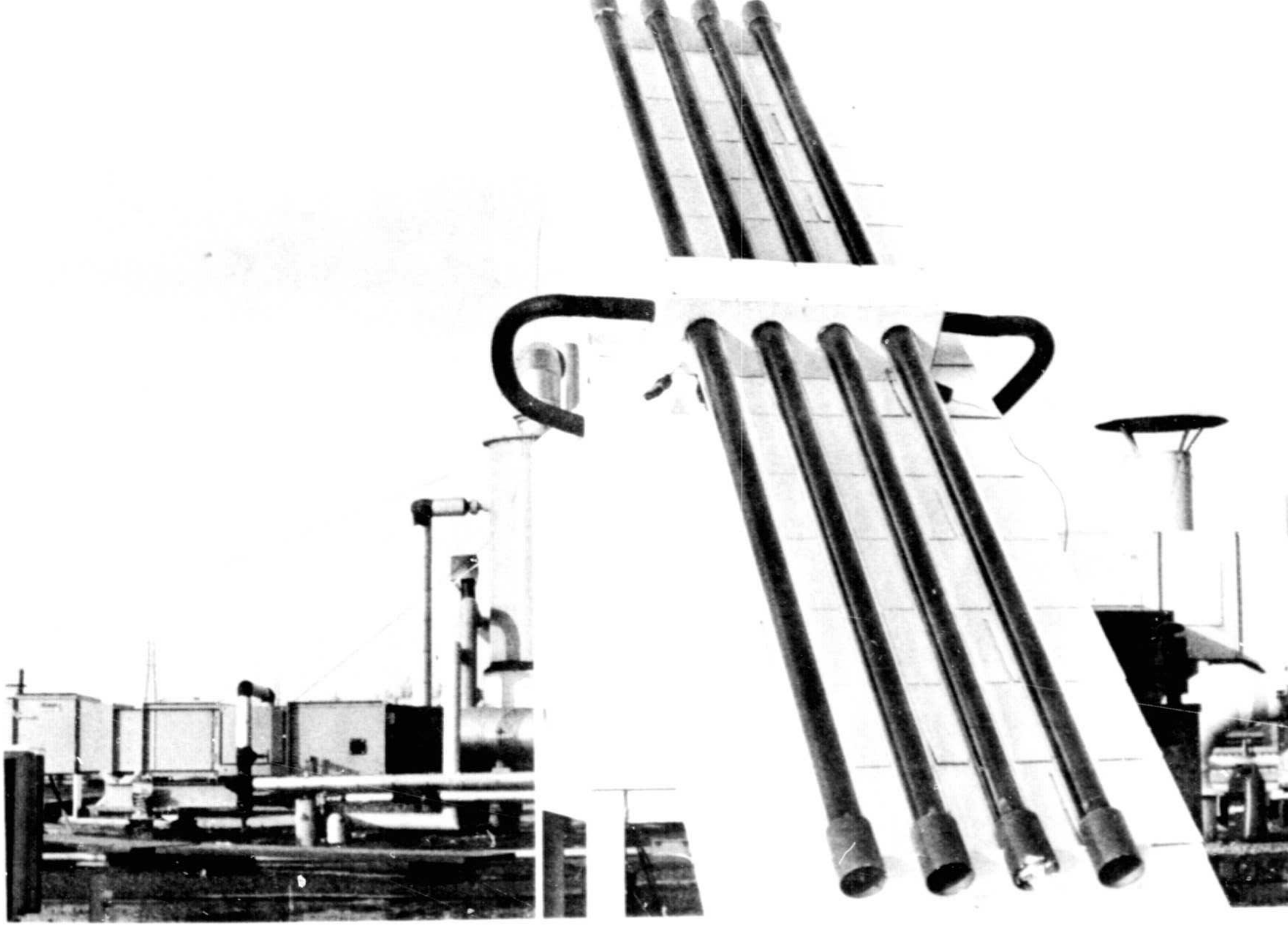

Figure 2. - Method of installation of glass tubular collector.

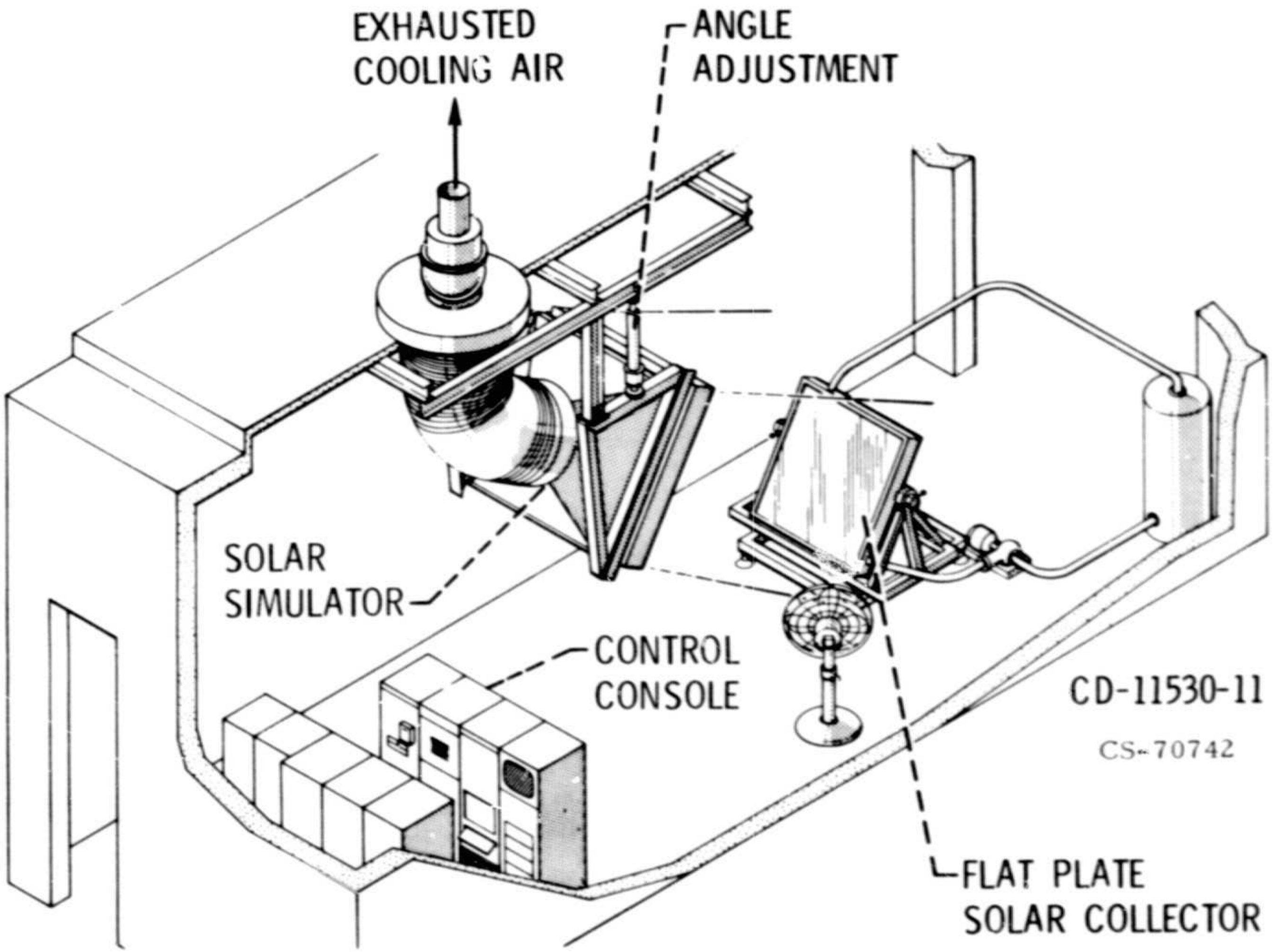

CD-11530-11

CS-70742

Figure 3. - Indoor test facility.

Figure 4. - Indoor facility used to experimentally determine solar collector performance.

E-8289

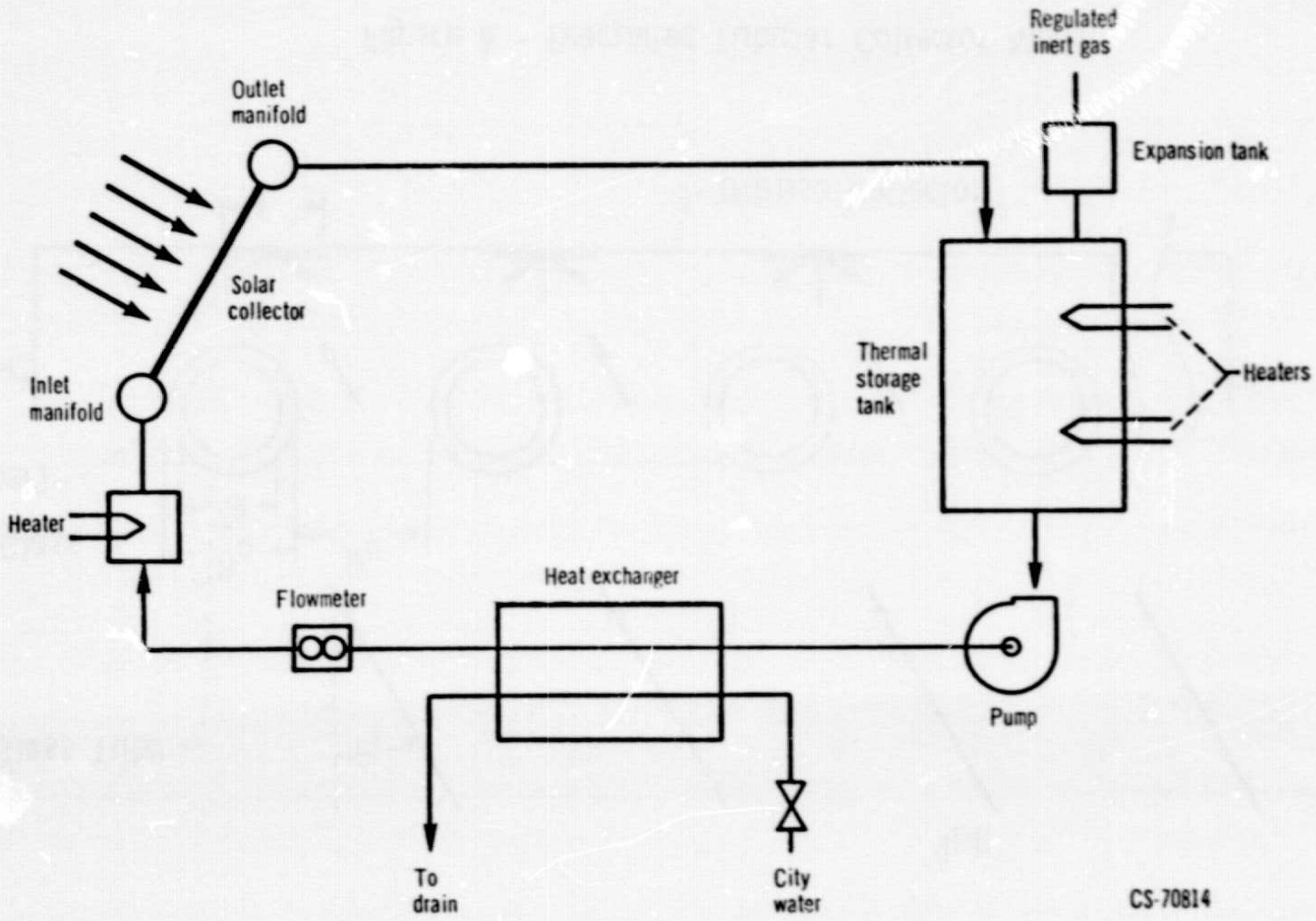

Figure 5. Schematic of liquid flow loop.

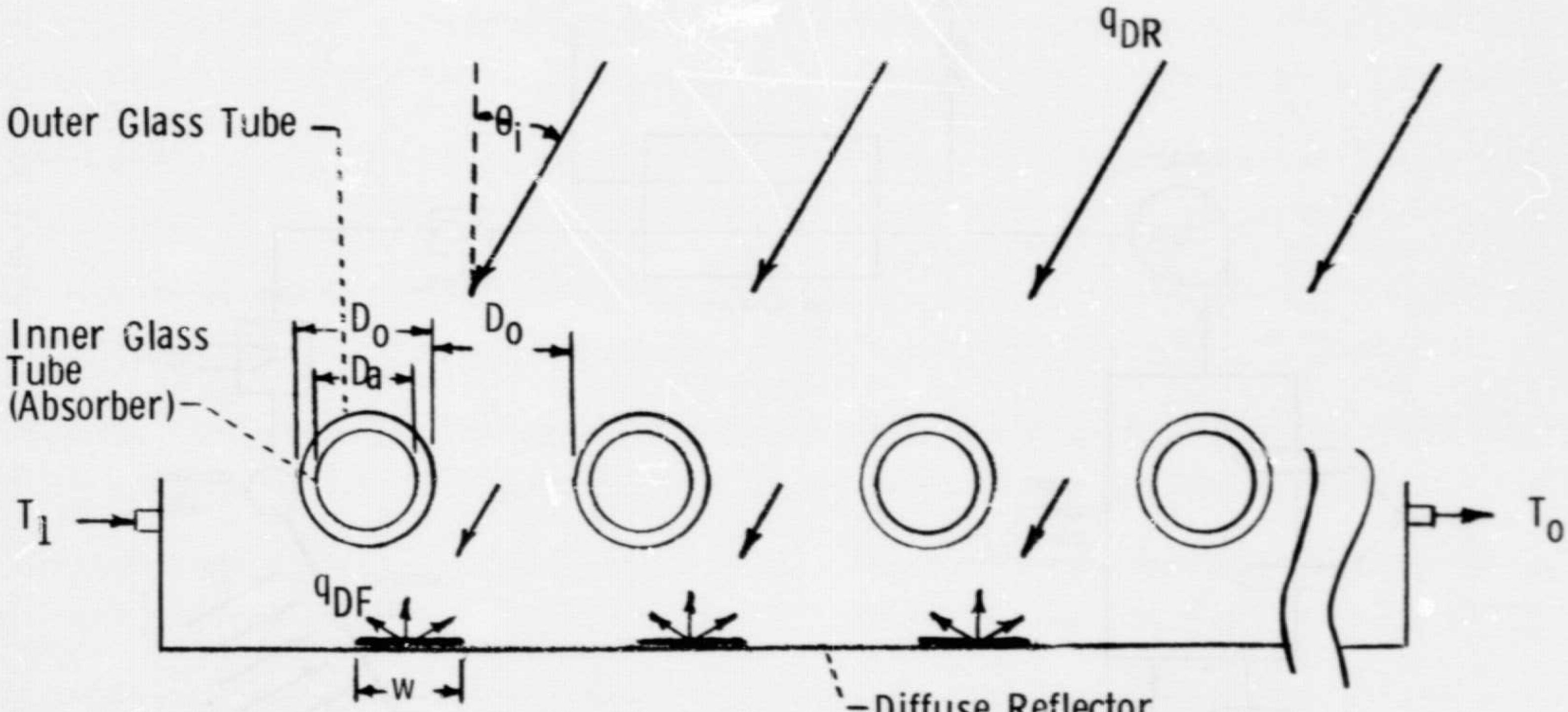

Figure 6. - Evacuated Tubular Collector Model

Figure 7. - Performance Curves of Evacuated Tubular Collector

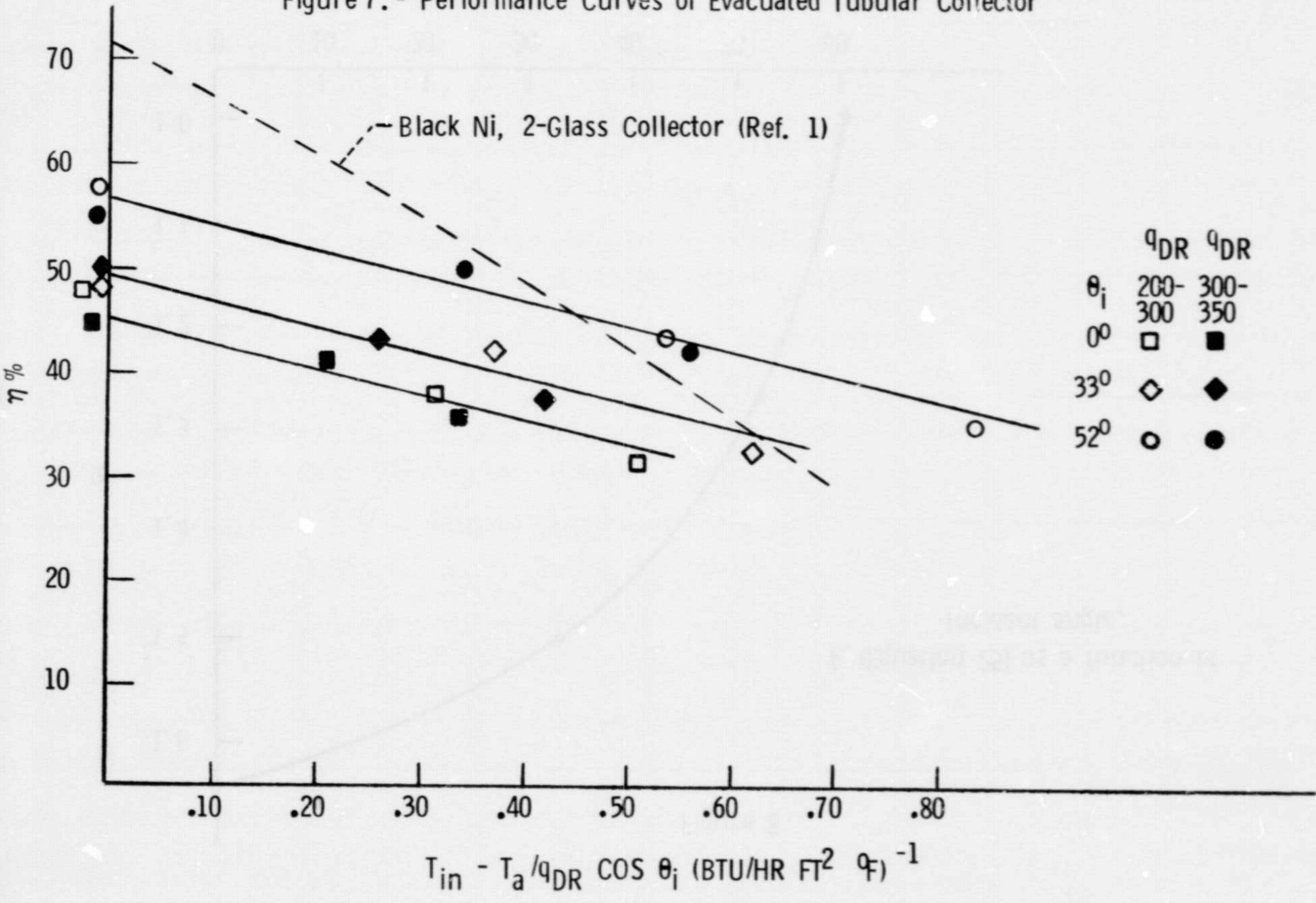

Figure 8

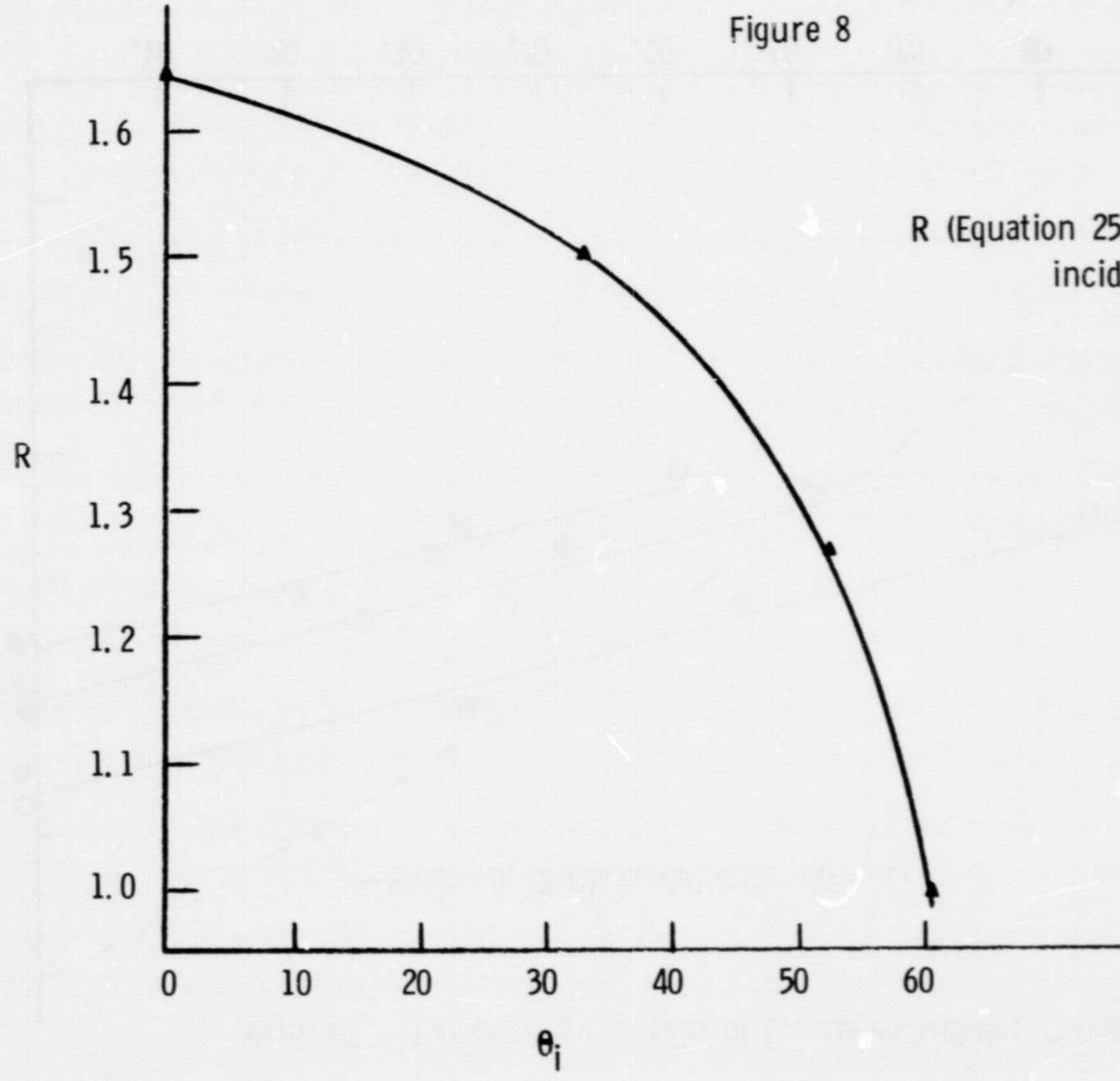

R (Equation 25) as a function of incident angle.

Figure 9. - All Day Collector Performance

For $T_1 = 200^0F$

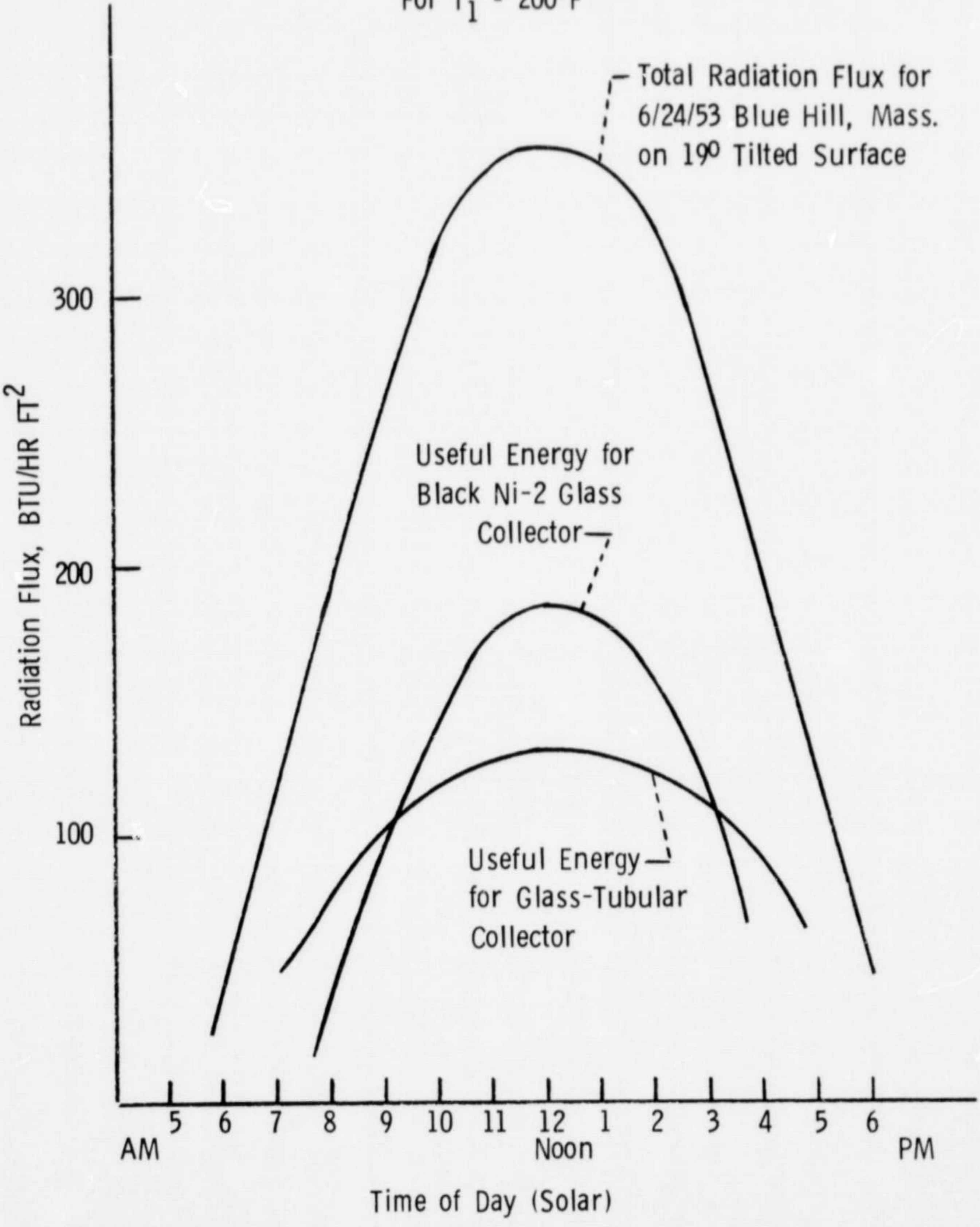

E-8289

NASA-Lewis